Hydrogen adsorption properties of in-situ synthesized Pt-decorated porous carbons templated from zeolite EMC-2

Zhuxian Yang*[,a], Quanli Jia[b], Binling Chen[a], Xinglong Gou[c], Yanqiu Zhu[a] and Yongde Xia*[,a]

[a] *College of Engineering, Mathematics and Physical Sciences, University of Exeter, Exeter EX4 4QF, United Kingdom*

[b] *Henan Key Laboratory of High Temperature Functional Ceramics, Zhengzhou University, Zhengzhou, 450052, PR China*

[c] *Chemical Synthesis and Pollution Control Key Laboratory of Sichuan Province, College of Chemistry and Chemical Engineering, China West Normal University, Nanchong 637000, PR China*

* Corresponding author. Email address: Z.Yang@exeter.ac.uk (ZX Yang); Tel: +44 1392 725345; Y.Xia@exeter.ac.uk (YD Xia); Tel: +44 1392 723683.

ABSTRACT

To increase the interaction between the adsorbed hydrogen and the adsorbent surface to improve the hydrogen storage capacity at ambient temperature, decorating the sorbents with metal nanoparticles, such as Pd, Ni, and Pt has attracted the most attention. In this work, Pt-decorated porous carbons were in-situ synthesized via CVD method using Pt-impregnated zeolite EMC-2 as template and their hydrogen uptake performance up to 20 bar at 77, 87, 298 and 308 K has been investigated with focus on the interaction between the adsorbed H_2 and the carbon matrix. It is found that the in-situ generated Pt-decorated porous carbons exhibit Pt nanoparticles with size of 2-4 nm homogenously dispersed in porous carbon, accompanied with observable carbon nanowires on the surface. The calculated H_2 adsorption heats at/near 77 K are similar for both the plain carbon (7.8 kJ mol^{-1}) and the Pt-decorated carbon (8.3 kJ mol^{-1}) at H_2 coverage of 0.08 wt.%, suggesting physisorption is dominated in both cases. However, the calculated H_2 adsorption heat at/near 298 K of Pt-decorated carbon is 72 kJ mol^{-1} at initial H_2 coverage, which decreases dramatically to 20.8 kJ mol^{-1} at H_2 coverage of 0.014 wt.%, levels to 17.9 at 0.073 wt.%, then gradually decreases to 2.6 kJ mol^{-1} at 0.13 wt.% and closes to that of the plain carbon at H_2 coverage above 0.13 wt.%. These results suggest that the introduce of Pt particles significantly enhances the interaction between the adsorbed H_2 and the Pt-decorated carbon matrix at lower H_2 coverage, resulting in an adsorption process consisting of chemisorption stage, mixed nature of chemisorption and physisorption stage along with the increase of H_2 coverage (up to 0.13 wt.%). However, this enhancement in the interaction is outperformed by the added weight of the Pt and the blockage and/or occupation of some pores by the Pt nanoparticles, which results in lower H_2 uptake than that of the plain carbon.

Keywords: porous carbon, hydrogen storage, adsorption heat, Pt, nanoparticles

Introduction

Due to the increasing demand of energy, the potential depleting of the currently widely used fossil fuels and the environmental issues caused by the use of them, it is urgent to find alternative energy sources and much effort has been devoted to the application of nanomaterials in the energy storage fields [1-8]. Hydrogen has been proposed as an ideal candidate for renewable energy, especially for mobile applications. Currently, the main issue with the use of hydrogen as a fuel is how to efficiently store hydrogen, given that the volumetric density of hydrogen at ambient pressure and room temperature is quite low. Among the four widely studied types of hydrogen storage methods, including high pressure hydrogen cylinder tanks, physisorption in porous materials including zeolites [9, 10], carbons [1-3, 11, 12], MOFs [1, 6, 13, 14], etc., chemisorption in metal hydrides ($LiBH_4$ and $AlBH_4$) [5, 15, 16] and chemisorption in chemical hydrides (such as ammonia borane**)** [17-19], physisorption in porous sorbents has the advantages of high energy efficiency because the hydrogen uptake and release is reversible via simple changes in pressure or temperature [20]. However, due to the weak interaction between the physisorbed hydrogen molecules and the sorbent surfaces, high hydrogen adsorption capacities can be achieved only at cryogenic temperatures and the hydrogen storage capacities at ambient temperature is quite low, i. e. far below 1 wt.%.

To increase the interaction between the molecular hydrogen and the adsorbent surface to improve the hydrogen storage capacity at ambient temperature, decorating the sorbents with metal nanoparticles, such as Pd, Ni, and Pt, has attracted the most attention so far, due to the reported hydrogen spillover effect [21]. There are reports demonstrating the enhancement of hydrogen storage capacity due to the spillover effect by decorating the carbon and other materials with metal nanoparticles [22-27]. However, there are also reports showing only slight or no enhancement in hydrogen storage capacities of Pt-doped activated carbon fibers

or templated carbons, Pd-doped carbon molecular sieves at room temperature [28-31]. The discrepancy could be due to the differences in the contact between the metal and the carbon receptor, metal particles, doping methods, nature and surface composition of the receptor, catalyst treatment etc., as all these factors can affect the enhancement by spillover [31-33].

The widely used method to prepare metal-decorated carbon materials is post-synthesis incipient wetness, in which the readily made carbon materials and the metal precursors are mixed in solution (solvent or water), followed by the evaporation of the solvent or water, and finally the resulting mixture is heat treated in inert atmosphere or vacuum to generated metal particles dispersed in carbon materials [24, 26, 27, 32, 34]. To explore other options for doping metals onto carbon, in situ doping has attracted increasing attention since it reduces the preparation steps, in which the metal reduction step was carried out during the carbonization process [20, 30, 35]. Here we report the in-situ synthesis of Pt-decorated porous carbons with high surface area and pore volume using Pt precursor impregnated EMC2 zeolite as template via chemical vapor deposition (CVD) process and further study on the H_2 storage up to 20 bar at 77, 87, 298 and 308 K with focus on the interaction between the adsorbed H_2 and the carbon matrix. Based on the H_2 uptake isotherms, the H_2 adsorption heat of the studied samples at/near 77 K and at/near 298 K were calculated.

Experimental

Sample preparation

The zeolite EMC-2 was synthesized based on reported method [36]. The microporous carbon materials (CEMC-2) were prepared via chemical vapor deposition (CVD) with zeolite EMC-2 as the template and acetonitrile as the carbon precursor at 1023 K. In brief, 1 g of zeolite was put in a tube furnace under Ar flow, and when the temperature reached 1023 K, Ar flow was replaced by a mixture flow of acetonitrile/Ar for 3 h, followed by cooling down under Ar

flow. The resulting carbon/zeolite composite was washed with 10% hydrofluoric acid several times, followed by refluxing with concentrated hydrochloric acid at 333 K to completely remove the zeolite framework. Finally, the resulting carbon materials were dried in an oven at 393 K overnight and named as CEMC. The Pt-doped carbons were prepared following the same procedure described for plain carbon except that zeolite EMCE-2 was replaced by the Pt-impregnated zeolite EMC-2. The Pt impregnated zeolite EMCE-2 was prepared as follows: a calculated amount of Pt precursor $Pt(NH_3)_4(NO_3)_2$ was dissolved in acetone/ethanol, then pre-dried zeolite CEMC-2 was added into the solution under stirring to achieve a 5 and 10 wt.% of Pt loading respectively. The mixture was stirred overnight at room temperature, followed by filtration, and drying in an oven to obtain Pt-impregnated EMC-2 samples. The Pt precursor $Pt(NH_3)_4(NO_3)_2$ was reduced to Pt metal by in-situ formed carbon which was carbonised from acetonitrile during the CVD process. The Pt-decorated carbon samples were named as Pt5CEMC and Pt10CEMC corresponding to the calculated 5 and 10 wt.% Pt loading on ECM-2 zeolite, respectively.

Sample characterization

The X-ray diffraction (XRD) measurement was carried out on a Bruker D8 Advance diffractometer working with CuKα (Ni-filtered) radiation λ = 0.15418 nm and a scanning step size of 2θ = 0.02°. The textural properties of samples were analyzed via N_2 sorption at 77 K with Quantachrome Autosorb iQ sorptometer. The surface area was calculated using the Brunauer-Emmett-Teller (BET) method based on the adsorption data in the partial pressure (P/P_0) range of 0.02-0.22. The total pore volume was determined from the amount of N_2 adsorbed at P/P_0 of *ca.* 0.99. The partial pressure range (P/P_0) 0.02 − 0.22 was selected for the calculation of surface area taking into account a previous report which indicates that low partial pressure range of P/P_0 0.01 − 0.05 will overestimate the surface area while the partial pressure range of P/P_0 0.1 − 0.3 can underestimate the surface area [37]. Micropore surface

area and micropore volume were obtained via t-plot analysis. The pore size distributions (PSD) were obtained using the non-local density functional theory (NLDFT) method for slit/cylinder pores using the software provided by Quantachrome. Scanning electron microscopy (SEM) images were obtained using a Philips XL-30 scanning electron microscope. Samples were mounted using a conductive carbon double-sided sticky tape on a sample holder. A thin (ca. 10 nm) coating of gold sputter was deposited onto the samples to reduce the effects of charging. Transmission electron microscopy (TEM) images were recorded on a JEOL 2000-FX electron microscope operating at 200 kV. TEM samples were prepared by dispersing carbon powder in acetone solvent, then dropping and spreading 1-2 drops on a holey carbon film supported on a grid. After vaporising the solvent, a dry carbon sample was retained on the grid.

H₂ uptake evaluation

The gravimetric analysis of hydrogen uptake capacity was performed using high-purity hydrogen (99.9999%) over the pressure range of $0 - 20$ bar with an Intelligent Gravimetric Analyzer (IGA-003, Hiden), which incorporates a microbalance capable of measuring weights with a resolution of ± 0.2 μg. The samples in the analysis chamber of the IGA-003 were evacuated to 10^{-10} bar and kept at 523 K overnight before measurement. The hydrogen uptake measurements were carried out at 77, 87, 298 and 308 K respectively. The high-purity hydrogen (99.9999%) was additionally purified by a molecular sieve filter and a liquid nitrogen trap. The H₂ adsorption heat Q_{st} at/near 77 K was calculated using hydrogen-adsorption isotherms measured at 77 and 87 K respectively, while the Q_{st} at/near 298 K was calculated using hydrogen-adsorption isotherms measured at 298 and 308 K respectively. For a certain adsorbed amount of H₂ (wt.%), the Q_{st} was calculated by applying the integral format of the Clausius–Clapeyron equation as follows [11, 38-40]:

$$lnP_2 - lnP_1 = \frac{Q_{st}}{R}(\frac{1}{T_1} - \frac{1}{T_2})$$

Where Q_{st} is the isosteric heat of adsorption, P and T are the pressure and temperature at certain H_2 coverage (wt.%) and R is the universal gas constant. It is worth mentioning that in addition to the method used in this study (from isotherms at different temperatures), isosteric heat of adsorption can be theoretically calculated by the Density Functional Theory [41-43] or the grand canonical Monte Carlo simulation [44].

Results and discussion

Fig. 1 shows the XRD patterns of the plain porous carbon CEMC and the Pt-decorated porous carbons Pt5CEMC and Pt10CEMC. The appearance of the two peaks at 2θ around 6º in sample CEMC indicates that the porous carbon has partially retained the structural pore ordering replicated from the template zeolite EMC-2 [45] and the absence of the peak at 2θ of 26º suggests the amorphous nature of the carbon. However, only one peak at 2θ around 6º can be observed for sample Pt5CEMC and the peak intensity decreases significantly. In addition, two extra weak and broad peaks appear at 2θ of 26º and 39.7º, corresponding to the (002) of graphitic carbon and the (111) of metal Pt respectively. In the case of sample Pt10CEMC, the XRD peak at 2θ around 6º is extremely weak and three extra peaks at 2θ of 26º, 39.7º and 46.3º are clearly observable, which are corresponding to the (002) of graphitic carbon, (111) and (200) of Pt respectively. The intensity of these peaks at 2θ of 26º and 39.7º of sample Pt10CEMC is much higher than that of Pt5CEMC due to the higher amount of metal Pt content. The disappearance of the peak/peaks at 2θ around 6º indicates that the Pt-decorated carbons lose some structural pore ordering replicated from the zeolite EMC-2 because of the introduction of the high level of metal Pt. Moreover, the intensity of the graphitic carbon peak at 2θ of 26º increase with the Pt content, suggesting that the introduction of the increased Pt level results in the improvement of the graphitic level of the

Pt-decorated carbons. In addition, the intensity of the XRD peaks of the Pt-containing samples at 39.7º and 46.3º for Pt metal increases with Pt loading content, but these peaks are in general broad, maybe due to the small particle size of the Pt metal in the samples.
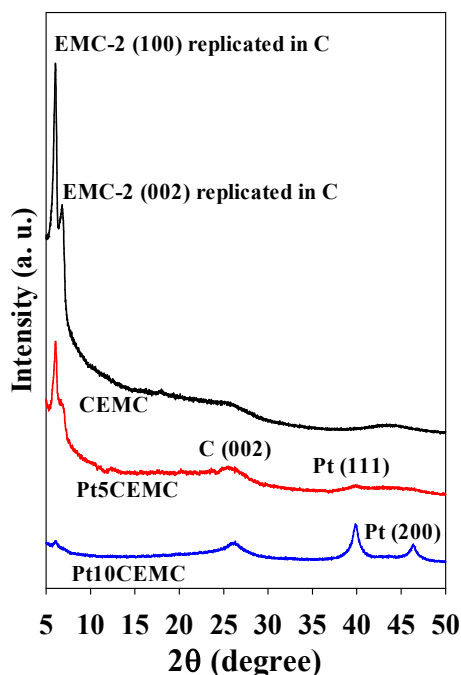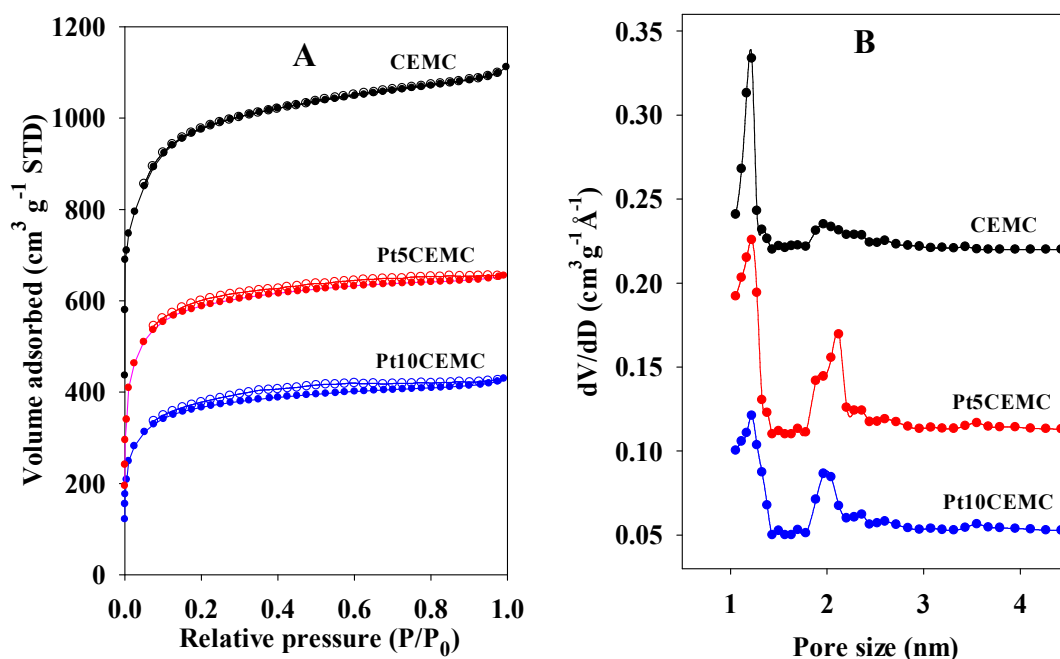

Fig. 1 − Powder XRD patterns of plain carbon (CEMC) and Pt-decorated carbons (Pt5CEMC and Pt10CEMC) templated from zeolite EMC-2 via CVD using acetonitrile as the carbon source at 1023 K.

The nitrogen sorption isotherms and pore size distribution of the plain carbon and Pt-decorated carbons are shown in Fig. 2A and their textural properties are summarised in Table 1. The plain carbon shows type I isotherms, typical for microporous materials while the two Pt-decorated carbons also show type I isotherms but with a very weak hysteresis loop, especially for Pt10CEMC, implying the presence of a small amount of mesopores. There is

significant adsorption at relative pressure $(P/P_0) < 0.02$ for all the samples indicating the presence of micropores. The plain carbon possesses high surface area of 3360 m^2 g^{-1} and pore volume of 1.91 cm^3 g^{-1}, with micropore surface area of 2838 m^2 g^{-1} and micropore volume of 1.24 cm^3 g^{-1}. The surface area decreases to 2049 and 1249 m^2 g^{-1} and the pore volume decreases to 1.06 and 0.66 cm^3 g^{-1} respectively for Pt5CEMC and Pt10CEMC. The pore size distribution (PSD) curves in Fig. 2B show that the plain carbon mainly possesses micropores with sizes centred at around 1.1 and 2.0 nm, with majority at 1.1 nm. In the case of Pt-decorated carbons, most pores are also centred at around 1.1 and 2.0 nm, but the contribution of pores around 2.0 nm is higher than that of the plain carbon. The possible reason could be that some small Pt particles enter the pores/pore channels of the carbons and/or are embedded in the carbon matrix, which occupy some pore channels and block some pores, especially micropores. As a result, the contribution of the micropores decreases and at the same time the contribution of the mesopores increases in the Pt-doped carbons as proved by the PSD. These observations are, on the one hand, due to the effect of added weight of the introduced Pt metal particles, and on the other hand, due to the fact that the pore structural ordering of the Pt-doped carbons deteriorates as evidenced by the disappearance or the weakening of the peaks at 2θ around 6º, which is one of the reasons that the specific surface area and pore volume of the Pt-containing porous carbons drop.

Fig. 2 − Nitrogen sorption isotherms (A) and pore size distribution curves (B) of plain carbon (CEMC) and Pt-decorated carbons (Pt5CEMC and Pt10CEMC) templated from zeolite EMC-2 via CVD using acetonitrile as the carbon source at 1023 K.

The SEM images of the plain porous carbon and the Pt-decorated porous carbons are presented in Fig. 3. Round plates are observed for all the samples as expected, showing that the carbons retain the morphology of the template. However, for the Pt-decorated porous carbons, the surfaces of some plates are covered with carbon wires (Fig. 3d and f). Fig. 3b and e reveal that only a very small amount of plates are covered with wires for Pt5CEMC, but more plates are covered for Pt10CEMC. The appearance of these wires indicates that the Pt metal particles act as a catalyst to produce carbon wires during the carbonization process. This morphology change of Pt-containing porous carbon samples, together with the pore blocking due to the presence of Pt particles, could result in the deteriorated pore structural ordering and the decrease of the surface area and pore volume for the Pt-containing samples.

| Sample	Surface area $(m^2\ g^{-1})$[a]	Pore volume $(cm^3\ g^{-1})$[a]	H_2 uptake $(wt.\%)$[b,c]
Table 1 − Textural properties and hydrogen uptake capacities of the plain porous carbon and the Pt-doped porous carbons templated from zeolite EMC-2 via CVD at 1023 K using acetonitrile as the carbon source.			
CEMC	3360 (2838)	1.71 (1.24)	6.33 (0.20)
Pt5CEMC	2047 (1664)	1.01 (0.70)	4.58 (0.18)
Pt10CEMC	1279 (1002)	0.66 (0.42)	3.99 (0.17)

[a] Values in parentheses are from micropores.

[b] H_2 uptake capacity at 77 K and 20 bar.

[c] Values in parentheses are H_2 uptake capacity at 298 K and 20 bar.
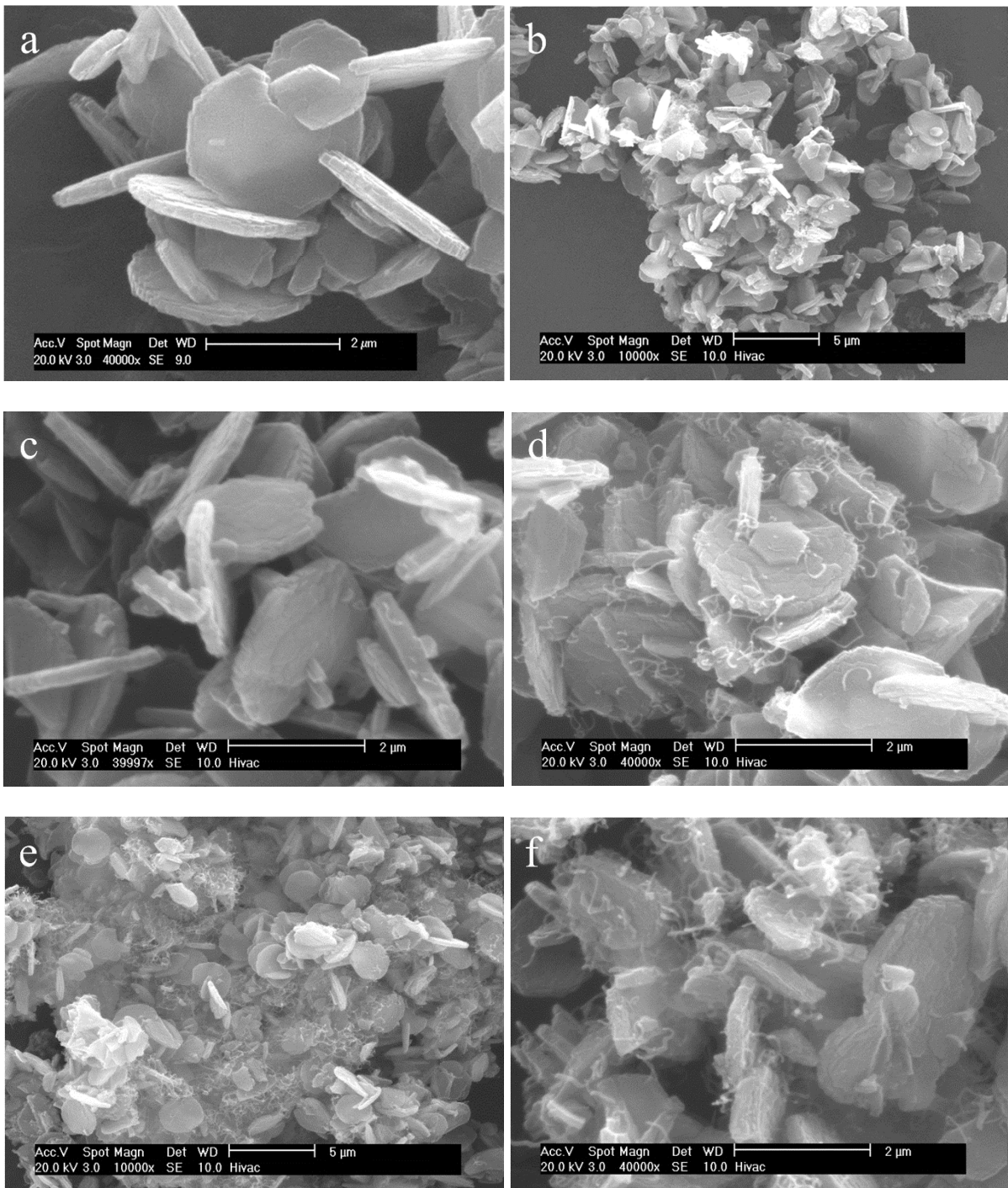
Fig. 3 ─ Representative SEM images of plain carbon (CEMC) (a) and Pt-decorated carbons Pt5CEMC (b-d) and Pt10CEMC (e-f) templated from zeolite EMC-2 via CVD using acetonitrile as the carbon source at 1023 K.

The TEM images of the Pt-decorated porous carbons in Fig. 4 show that the Pt nanoparticles are well dispersed in the carbon matrix for both samples. According to the particle size distribution histograms shown in Fig. 5, for Pt5CEMC, most of the Pt nanoparticles are in the range of 1-4 nm, and centred at 2-3 nm; while for Pt10CEMC, most of the Pt nanoparticles are in the range of 2-5 nm, and centred at 2.5-4 nm. The particle sizes are comparable to those obtained by post-synthesis incipient wetness method [24], and roughly consistent with the particle size derived from XRD in Fig. 1 from Scherer's equation. Sample Pt10CEMC exhibits higher constitution of particle sizes larger than 3 nm compared to Pt5CEMC, which is reasonable as nanoparticles intend to agglomerate at higher content. In addition, as expected, the Pt particles are denser in Pt10CEMC than that in Pt5CEMC, which is in good agreement with the XRD results in Fig. 1 that the intensity of the XRD peaks at 39.7º and 46.3º for Pt metal increases with Pt loading content.
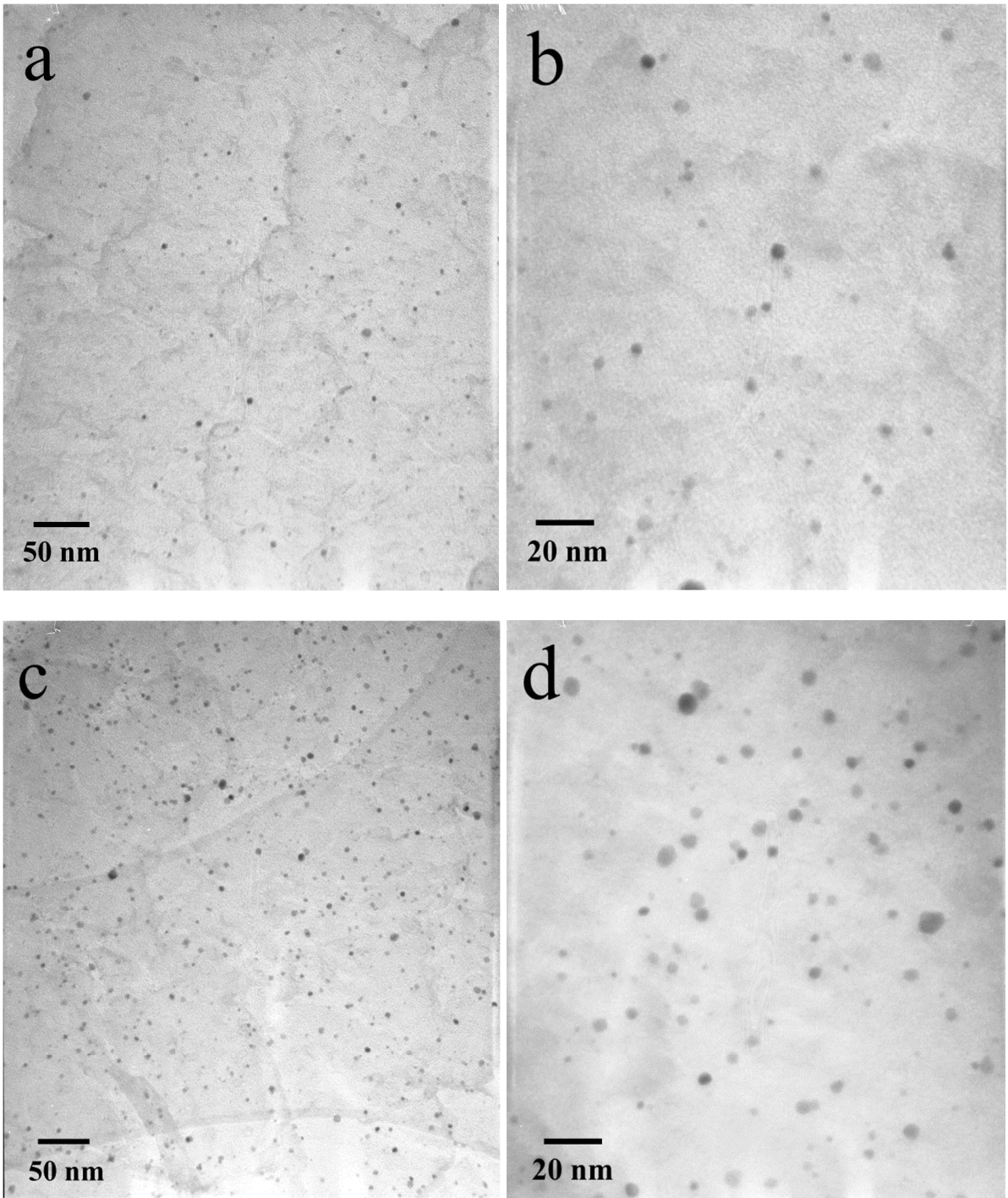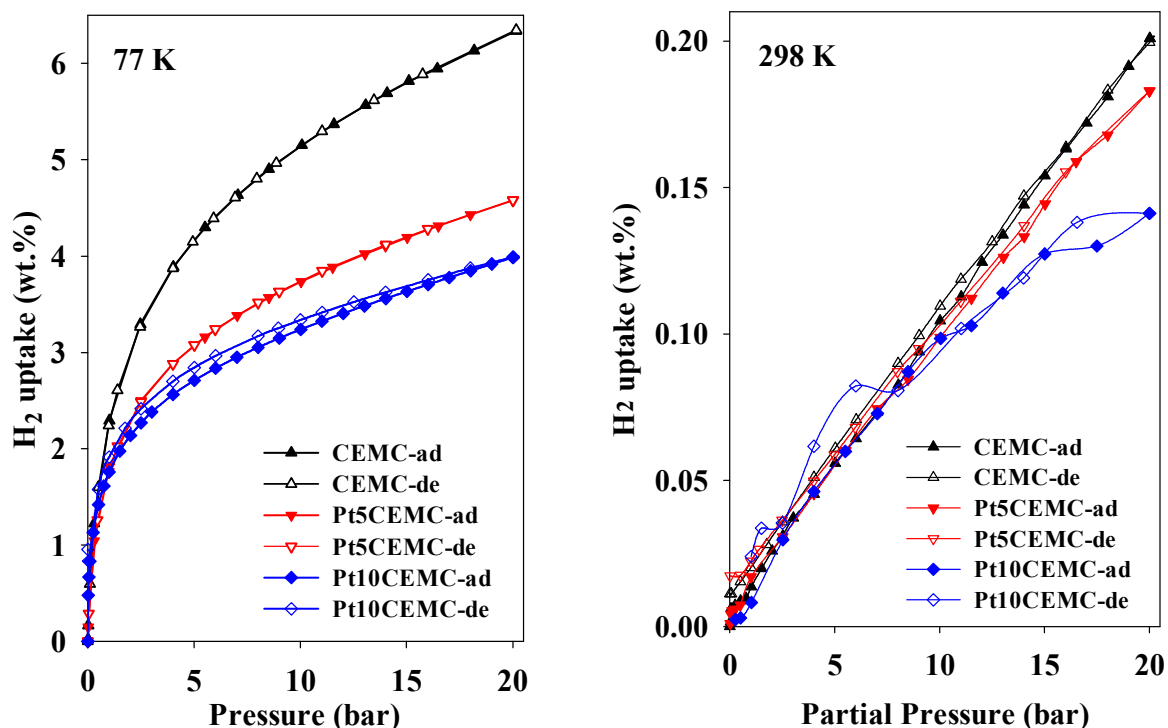
Fig. 4 — Representative TEM images of Pt-decorated carbons Pt5CEMC (a, b) and Pt10CEMC (c, d) templated from zeolite EMC-2 via CVD using acetonitrile as the carbon source at 1023 K.
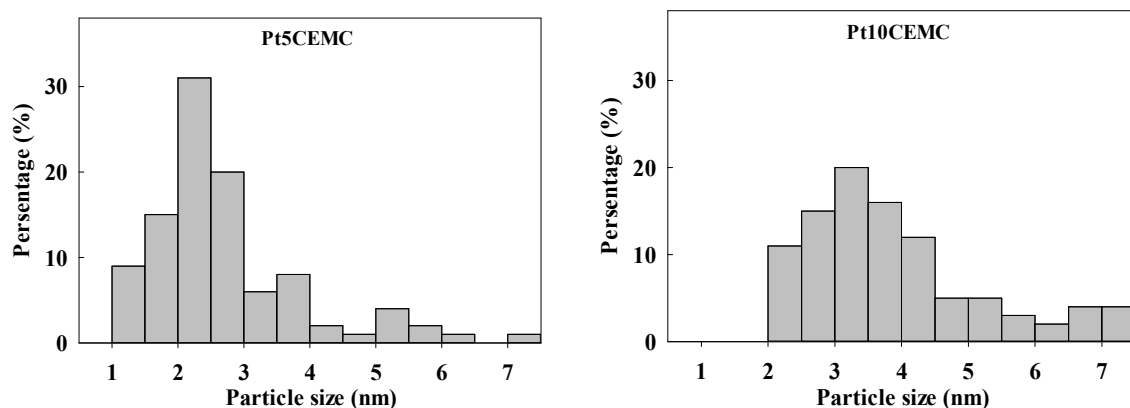
Fig. 5 — Metal Pt particle size distribution histograms of the Pt-decorated porous carbons Pt5CEMCW and Pt10CEMCW.

Fig. 6 shows the H_2 uptake isotherms of the plain porous carbon and the Pt-decorated porous carbons up to 20 bar at 77 and 298 K respectively. The hydrogen uptake isotherms were evaluated based on the measured bulk density of 1.5 g cm^{-3} for the samples, and the H_2 density of 0.04 g/cm^3 was used for buoyancy correction of the adsorbed H_2 [46]. At 77 K, both the plain porous carbon and sample Pt5CEMC show reversible isotherms without any hysteresis loop, indicating that the H_2 adsorption is completely reversible. However, Pt10CEMC shows a weak hysteresis loop, implying the H_2 adsorption is mostly reversible. At 77 K and 20 bar, the H_2 uptake capacity of the plain porous carbon is 6.33 wt.%, which is comparable to the reported values for templated porous carbon with similar high specific surface area and pore volume [11]. However, the H_2 uptake values decrease to 4.58 and 3.99 wt.% for the Pt-doped porous carbon samples Pt5CEMC and Pt10CEMC respectively.

15

Fig. 6 － Hydrogen uptake capacities at 77 and 298 K of plain porous carbon (CEMC) and Pt-doped porous carbons Pt5CEMC and Pt10CEMC templated from zeolite EMC-2 via CVD using acetonitrile as the carbon source at 1023 K.

At 298 K, both the plain porous carbon and sample Pt5CEMC show roughly reversible isotherms with very weak hysteresis loop, except that at very low pressure less than 0.6 bar, the H_2 desorption values are much higher than those adsorption ones for sample Pt5CEMC. In addition, Pt10CEMC exhibits some weak hysteresis loops due to the jumping of measured values in the desorption branch, implying the irreversible performance of H_2 adsorption. At both 77 and 298 K, the isotherms of Pt10CEMC are different from that of the plain carbon and Pt5CEMC by the appearance of the hysteresis loops (i.e. the H_2 adsorption is not fully reversible). This is because part of the H_2 was chemically adsorbed (chemical reaction occurred) by Pt10CEMC due to the relatively high Pt content, which was not desorbed upon

decrease of the pressure. In addition, chemical adsorption involves activation energy means high temperature can enhance chemical adsorption, which explains that the hysteresis loops at 298 K are more significant than that at 77 K for Pt10CEMC. Therefore, it is clear both the Pt content and the temperature play a role in the chemisorption of H_2. The H_2 uptake capacities at 298 K and 20 bar are 0.20, 0.18 and 0.17 wt.% for the plain porous carbon, Pt5CEMC and Pt10ECMC respectively. Therefore, regardless of the H_2 uptake measurement temperatures, the plain carbon shows the highest H_2 uptake capacity among the three samples. The introduction of the Pt nanoparticles into porous carbons results in the decrease of the H_2 uptake capacities, which may be due to the added weight of the metal Pt, partial pore blocking and/or pore occupation by the Pt nanoparticles in the carbons. The result obtained at 77 K is in agreement with reports that at cryogenic temperatures there is no spillover effect and the H_2 uptake capacity is determined by the specific surface area and pore volume of the studied samples [27, 34]. However, the H_2 uptake results obtained at 298 K is contrary to the report in which Pt was introduced into porous carbon templated from zeolite EMC-2 by post-synthesis incipient wetness method [24], which showed significant H_2 adsorption enhancement due to the H_2 spillover effect at 298 K. The possible reason that no enhancement in H_2 uptake occurs in this study could be due to the different introducing method of Pt nanoparticles, in which the Pt metal ions reduction was in-situ carried out during the carbonization step. As revealed by the SEM images, part of the surface of the Pt-decorated porous carbons are covered with some wires, indicating that the Pt nanoparticles were acting as a catalyst to produce carbon wires, which might have deactivated their activity for H_2 spillover effect.

Regarding sample Pt10CEMC, the presence of the hysteresis loop and the jumping of measured values in its H_2 desorption branch could be due to the chemisorption of H_2 given the higher metal Pt content. Because of the jumping of measured points of the desorption of

17

branch and low H_2 adsorption capacity, only the plain porous carbon and sample Pt5CEMC were further measured at 87 and 308 K respectively up to 20 bar in order to calculate the H_2 adsorption heat using the Clausius–Clapeyron equation described in the experimental part. The H_2 uptake isotherms of the plain porous carbon and sample Pt5CEMC at various temperatures are shown in Fig. 7, and the inserts in Fig. 7 are the zoomed H_2 uptake isotherms measured at 298 and 308 K due to the low uptake capacities at these temperatures. Both the plain porous carbon and the Pt-decorated porous carbon show the same trend of H_2 adsorption that the H_2 uptake capacities decrease with increasing temperatures, and the H_2 uptake capacities at 20 bar of the plain porous carbon are higher than that of the Pt-decorated porous carbon at all studied temperatures. These results indicate that physisorption is dominated in the H_2 uptake for both the plain porous carbon and the Pt-decorated porous carbon.
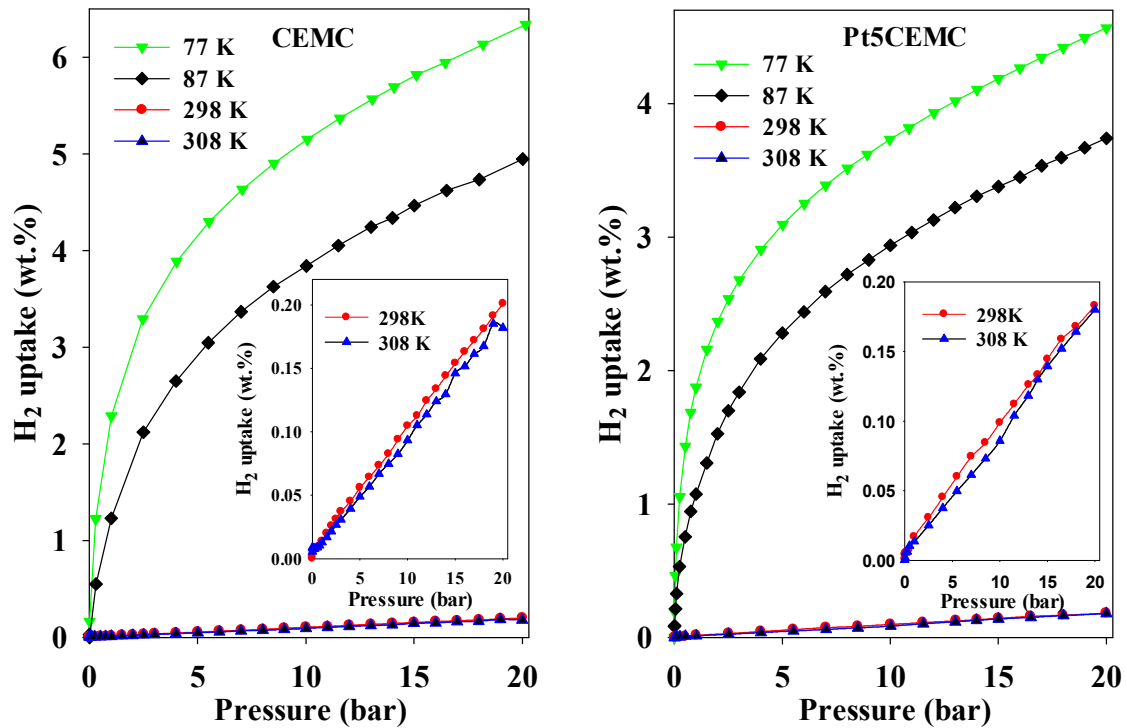
Fig. 7 － Hydrogen uptake capacities of plain carbon CEMC and Pt5CEMC measured at 77, 87, 298 and 308 K. The inserts are the zoomed H_2 uptake isotherms measured at 298 and 308 K.

The H_2 uptake isotherms measured at 77 and 87 K were used to calculate the H_2 adsorption heat at/near cryogenic temperature and those at 298 and 308 K were used for the calculation of the H_2 adsorption heat at/near ambient temperature for both the plain porous carbon and the Pt-decorated porous carbon using the Clausius–Clapeyron equation. The H_2 adsorption heats at/near cryogenic and ambient temperatures are shown in Fig. 8. At/near cryogenic temperature, the initial H_2 adsorption heats are 7.8 and 8.3 kJ mol^{-1} at H_2 coverage of 0.08 wt.% for the plain porous carbon and sample Pt5CEMC respectively, which are typical for physisorption and comparable to previous report [11]. The adsorption heat of the plain porous carbon decreases to 5.0 kJ mol^{-1} with the increase of H_2 coverage up to 2.6 wt.%, and it roughly remains at around 5.0 kJ mol^{-1} when the H_2 coverage is up to 5.0 wt.%. In the case of Pt5CEMC, the adsorption heat also decreases with the increase of H_2 coverage up to 1.3 wt.%, and then it decreases linearly with the increasing H_2 coverage. The adsorption heat of the Pt-decorated carbon Pt5CEMC is slightly higher than that of the plain carbon up to H_2 coverage of 2.6 wt.%, implying the slight enhancement of interaction between the adsorbed H_2 and the surface of the Pt-decorated carbon. However, this slight enhancement in the interaction between the H_2 and the carbon is outperformed by the added weight of the Pt and the blockage and/or occupation of some pores by the Pt nanoparticles, therefore the Pt-decorated carbon exhibits less H_2 storage capacity.

19
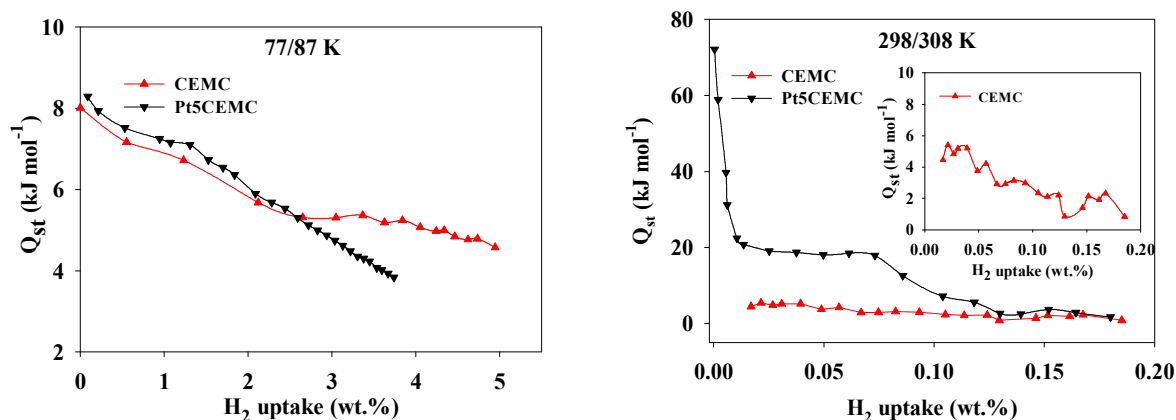
Fig. 8 － Isosteric heat of adsorption (Q_{st}) as a function of the amount of hydrogen adsorbed on plain porous carbon CEMC and Pt5CEMC at/near cryogenic temperature calculated from isotherms measured at 77 and 87 K and at/near room temperature calculated from isotherms measured at 298 and 308 K.

At/near ambient temperature (298/308 K), the H_2 adsorption heat of Pt5CEMC is much higher than that of the plain porous carbon in the whole measured H_2 coverage. The initial H_2 adsorption heat of the plain porous carbon is around 5.4 kJ mol^{-1}, which gradually decreases with the increase of the H_2 coverage and the adsorption heat for this plain carbon is 0.9 kJ mol^{-1} at the H_2 coverage of 0.18 wt.%. These values are slightly lower than that obtained at cryogenic temperature as expected. However, the Pt-decorated porous carbon sample Pt5CEMC shows a complete different scenario where H_2 adsorption heat of 72 kJ mol^{-1} is observed at the initial H_2 coverage (close to 0), which decreases dramatically to 20.8 kJ mol^{-1} at H_2 coverage of 0.014 wt.%, and levels to 17.9 at 0.073 wt.%. Then it gradually decreases to 2.6 kJ mol^{-1} at 0.13 wt.% and closes to that of the plain carbon at H_2 coverage above 0.13 wt.%. A H_2 adsorption heat of 72 kJ mol^{-1} with no doubt indicates that chemisorption or chemical reaction occurs due to the presence of metal Pt particles in the carbon sample.

20

However, this chemisorption only contributes to negligible H_2 adsorption given the low H_2 coverage (below 0.014 wt.%). This could be because that some of the Pt nanoparticles might have been embedded inside the porous carbon matrix, which makes them less accessible and some could have been deactivated by catalysing the formation of carbon wires (as shown in the SEM images in Fig. 3). At H_2 coverage from 0.014 wt.% to 0.073 wt.%., the H_2 uptake of sample Pt5CEMC behaves in a mixed nature of chemisorption and physisorption, but at H_2 coverage from 0.073 to 0.13 wt.%, it is dominated by physisorption with relatively stronger interaction between the H_2 molecules and the carbon materials due to the presence of Pt nanoparticles. At H_2 coverage higher than 0.13 wt.%, the exposed Pt nanoparticles in the sample may have been consumed and surrounded by adsorbed H_2 molecules, leading to an adsorption heat similar to that of plain carbon. Physical adsorption is dominated at low temperature (77 K) while both chemical and physical adsorptions are observed at high temperature (298 K) for sample Pt5CEMC. As discussed above, for sample Pt10CEMC2 both the Pt content and the sorption temperature play a role in the chemisorption of H_2 which requires activation energy. Given the relatively low Pt content in sample Pt5CEMC and low temperature at 77 K which may not provide enough activation energy for chemisorption, only physisorption is possible. However, at the temperature of 298 K, the activation energy is not an issue and the chemisorption of H_2 takes place. Based on the above results and discussion, it can be concluded that at/near 298 K, the introduction of Pt does significantly enhance the interaction between the adsorbed H_2 and the Pt-decorated carbon matrix, resulting in an adsorption process consisting of chemisorption stage, mixed nature of chemisorption and physisorption stage and physisorption stage along with the increase of H_2 coverage. However, this enhancement in the interaction between the adsorbed H_2 and the carbon matrix is outperformed by the added weight of the Pt and the blockage and/or occupation of some pores by the Pt nanoparticles, which results in lower H_2 uptake than that of the plain carbon.

Conclusions

Based on the above results, we can draw the following conclusions. The in-situ synthesis strategy can produce Pt-doped carbon with well dispersed Pt nanoparticles in the sizes of 1-4 nm or 2-5 nm with Pt loading of 5 and 10 wt.% respectively. The H_2 adsorption heats calculated from the isotherms of plain carbon and Pt-decorated carbon at 77, 87, 298 and 308 K indicate that at lower H_2 coverage, the introduce of Pt slightly increases the hydrogen adsorption heat at/near 77 K, but significantly increases the hydrogen adsorption heat at/near 298 K implying the enhancement in the interaction between the adsorbed H_2 and the Pt-decorated carbon matrix. This enhancement leads to the H_2 adsorption process consisting of chemisorption stage, mixed nature of chemisorption and physisorption stage and physisorption stage along with the increase of H_2 coverage. However, despite the enhancement in the interaction between the adsorbed H_2 and the carbon matrix, the H_2 uptake of the Pt-decorated carbon is lower than that of the plain carbon since other factors, such as the added weight of the Pt and the blockage and/or occupation of some pores by the Pt nanoparticles outperform the enhancement.

REFERENCES

[1] Thomas KM. Hydrogen adsorption and storage on porous materials. Catal Today 2007;120:389-98.

[2] de la Casa-Lillo MA, Lamari-Darkrim F, Cazorla-Amoros D, Linares-Solano A. Hydrogen storage in activated carbons and activated carbon fibers. J Phys Chem B 2002;106:10930-4.

[3] Panella B, Hirscher M, Roth S. Hydrogen adsorption in different carbon nanostructures. Carbon 2005;43:2209-14.

[4] Mousavi-Kamazani M, Zarghami Z, Salavati-Niasari M. Facile and novel chemical synthesis, characterization, and formation mechanism of copper sulfide (Cu_2S, Cu_2S/CuS, CuS) nanostructures for increasing the efficiency of solar cells. J Phys Chem C 2016;120:2096-108.

[5] Davids MW, Lototskyy M, Malinowski M, van Schalkwyk D, Parsons A, Pasupathi S, et al. Metal hydride hydrogen storage tank for light fuel cell vehicle. Int J Hydrogen Energy 2019;44:29263-72.

[6] Hardy B, Tamburello D, Corgnale C. Hydrogen storage adsorbent systems acceptability envelope. Int J Hydrogen Energy 2018;43:19528-39.

[7] Ramimoghadam D, Gray EM, Webb CJ. Review of polymers of intrinsic microporosity for hydrogen storage applications. Int J Hydrogen Energy 2016;41:16944-65.

[8] Banerjee P, Thapa R, Rajkamal A, Chandrakumar KRS, Das GP. First-principles identification of the origin for higher activity of surface doped carbon nanohorn: Impact on hydrogen storage. Int J Hydrogen Energy 2019;44:23196-209.

[9] Zecchina A, Bordiga S, Vitillo JG, Ricchiardi G, Lamberti C, Spoto G, et al. Liquid hydrogen in protonic chabazite. J Am Chem Soc 2005;127:6361-6.

[10] Arean CO, Delgado MR, Palomino GT, Rubio MT, Tsyganenko NM, Tsyganenko AA, et al. Thermodynamic studies on hydrogen adsorption on the zeolites Na-ZSM-5 and K-ZSM-5. Microporous Mesoporous Mater 2005;80:247-52.

[11] Yang ZX, Xia YD, Mokaya R. Enhanced hydrogen storage capacity of high surface area zeolite-like carbon materials. J Am Chem Soc 2007;129:1673-9.

[12] Xia YD, Yang ZX, Gou XL, Zhu YQ. A simple method for the production of highly ordered porous carbon materials with increased hydrogen uptake capacities. Int J Hydrogen Energy 2013;38:5039-52.

[13] Rowsell JLC, Millward AR, Park KS, Yaghi OM. Hydrogen sorption in functionalized metal-organic frameworks. J Am Chem Soc 2004;126:5666-7.

[14] Yang SJ, Im JH, Nishihara H, Jung H, Lee K, Kyotani T, et al. General relationship between hydrogen adsorption capacities at 77 and 298 K and pore characteristics of the porous adsorbents. J Phys Chem C 2012;116:10529-40.

[15] Sakintuna B, Lamari-Darkrim F, Hirscher M. Metal hydride materials for solid hydrogen storage: A review. Int J Hydrogen Energy 2007;32:1121-40.

[16] Rusman NAA, Dahari M. A review on the current progress of metal hydrides material for solid-state hydrogen storage applications. Int J Hydrogen Energy 2016;41:12108-26.

[17] Langmi HW, McGrady GS. Non-hydride systems of the main group elements as hydrogen storage materials. Coord Chem Rev 2007;251:925-35.

[18] Hamilton CW, Baker RT, Staubitz A, Manners I. B-N compounds for chemical hydrogen storage. Chem Soc Rev 2009;38:279-93.

[19] Peng B, Chen J. Ammonia borane as an efficient and lightweight hydrogen storage medium. Energ Environ Sci 2008;1:479-83.

[20] Alam N, Mokaya R. Characterisation and hydrogen storage of Pt-doped carbons templated by Pt-exchanged zeolite Y. Micropor Mesopor Mater 2011;142:716-24.

[21] Srinivas ST, Rao PK. Direc observation of hydrogen spillover on carbon-supported platinum and its influence on the hydrogenation of benzene. J Catal 1994;148:470-7.

[22] Zielinski M, Wojcieszak R, Monteverdi S, Mercy M, Bettahar MM. Hydrogen storage in nickel catalysts supported on activated carbon. Int J Hydrogen Energy 2007;32:1024-32.

[23] Parambhath VB, Nagar R, Ramaprabhu S. Effect of nitrogen doping on hydrogen storage capacity of palladium decorated craphene. Langmuir 2012;28:7826-33.

[24] Wang LF, Yang RT. Molecular hydrogen and spiltover hydrogen storage on high surface area carbon sorbents. Carbon 2012;50:3134-40.

[25] Rossetti I, Ramis G, Gallo A, Di Michele A. Hydrogen storage over metal-doped activated carbon. Int J Hydrogen Energy 2015;40:7609-16.

[26] Baca M, Cendrowski K, Kukulka W, Bazarko G, Moszynski D, Michalkiewicz B, et al. A comparison of hydrogen storage in Pt, Pd and Pt/Pd alloys loaded disordered mesoporous hollow carbon spheres. Nanomaterials 2018;8:639

[27] Zhao W, Luo L, Chen T, Li Z, Zhang Z, Wang H, et al. Synthesis and characterization of Pt-N-doped activated biocarbon composites for hydrogen storage. Compos B Eng 2019;161:464-72.

[28] Takagi H, Hatori H, Yamada Y. Hydrogen adsorption/desorption property of activated carbon loaded with platinum. Chem Lett 2004;33:1220-1.

[29] Jain P, Fonseca DA, Schaible E, Lueking AD. Hydrogen uptake of platinum-doped graphite nanoribers and stochastic analysis of hydrogen spillover. J Phys Chem C 2007;111:1788-800.

[30] Oh H, Gennett T, Atanassov P, Kurttepeli M, Bals S, Hurst KE, et al. Hydrogen adsorption properties of platinum decorated hierarchically structured templated carbons. Micropor Mesopor Mater 2013;177:66-74.

[31] Giasafaki D, Charalambopoulou G, Tampaxis C, Stubos A, Steriotis T. Hydrogen sorption properties of Pd-doped carbon molecular sieves. Int J Hydrogen Energy 2014;39:9830-6.

[32] Stuckert NR, Wang LF, Yang RT. Characteristics of hydrogen storage by spillover on Pt-Doped carbon and catalyst-bridged metal organic framework. Langmuir 2010;26:11963-71.

[33] Tsao CS, Tzeng YR, Yu MS, Wang CY, Tseng HH, Chung TY, et al. Effect of catalyst size on hydrogen storage capacity of Pt-Impregnated active carbon via spillover. J Phys Chem Lett 2010;1:1060-3.

[34] Zhao W, Fierro V, Zlotea C, Izquierdo MT, Chevalier-Cesar C, Latroche M, et al. Activated carbons doped with Pd nanoparticles for hydrogen storage. Int J Hydrogen Energy 2012;37:5072-80.

[35] Saha D, Deng SG. Hydrogen adsorption on ordered mesoporous carbons doped with Pd, Pt, Ni, and Ru. Langmuir 2009;25:12550-60.

[36] Delprato F, Delmotte L, Guth JL, Huve L. Synthesis of new silica-rich cubic and hexagonal faujasites using crown-ether-based supramolecules as templates. Zeolites 1990;10:546-52.

[37] Matsuoka K, Yamagishi Y, Yamazaki T, Setoyama N, Tomita A, Kyotani T. Extremely high microporosity and sharp pore size distribution of a large surface area carbon prepared in the nanochannels of zeolite Y. Carbon 2005;43:876-9.

[38] Knight EW, Gillespie AK, Prosniewski MJ, Stalla D, Dohnke E, Rash TA, et al. Determination of the enthalpy of adsorption of hydrogen in activated carbon at room temperature. Int J Hydrogen Energy 2020;45:15541-52.

[39] Xia YD, Mokaya R, Walker GS, Zhu YQ. Superior CO_2 adsorption capacity on N-doped, high-surface-area, microporous carbons templated from zeolite. Adv Energy Mater 2011;1:678-83.

[40] Whittaker PB, Wang XL, Regenauer-Lieb K, Chua HT. Predicting isosteric heats for gas adsorption. Phys Chem Chem Phys 2013;15:473-82.

[41] Liu ZY, Liu S, Er S. Hydrogen storage properties of Li-decorated B2S monolayers: A DFT study. Int J Hydrogen Energy 2019;44:16803-10.

[42] Rungnim C, Faungnawakij K, Sano N, Kungwan N, Namuangruk S. Hydrogen storage performance of platinum supported carbon nanohorns: A DFT study of reaction mechanisms, thermodynamics, and kinetics. Int J Hydrogen Energy 2018;43:23336-45.

[43] Wang JF, Rong YF, Han T, Ma LJ, Jia JF, Wu HS. The optimal adsorption pathway of H-2 molecules on Ti-Acetylene/ethylene compounds: A DFT study. Int J Hydrogen Energy 2020;45:2105-18.

[44] Du ZY, Nie XH, Deng S, Zhao L, Li SJ, Zhang Y, et al. Comparative analysis of calculation method of adsorption isosteric heat: Case study of CO_2 capture using MOFs. Microporous Mesoporous Mater 2020;298:110053.

[45] Gaslain FOM, Parmentier J, Valtchev VP, Patarin J. First zeolite carbon replica with a well resolved X-ray diffraction pattern. Chem Commun 2006:991-3.

[46] Kowalczyk P, Holyst R, Terzyk AP, Gauden PA. State of hydrogen in idealized carbon slitlike nanopores at 77 K. Langmuir 2006;22:1970-2.